Extreme Geomagnetic Disturbances (GMDs) Observed in Eastern Arctic Canada: Occurrence Characteristics and Solar Cycle Dependence

Mark J. Engebretson[1], Lily Yang[1], Erik S. Steinmetz[1], Vyacheslav A. Pilipenko[2], Mark B. Moldwin[3], Brett A. McCuen[3], Martin G. Connors[4], James M. Weygand[5], Colin L. Waters[6], Yukitoshi Nishimura[7], Larry R. Lyons[8], and Christopher T. Russell[5]

[1] Department of Physics, Augsburg University, Minneapolis, MN
[2] Institute of Physics of the Earth, Moscow, Russia
[3] Department of Climate and Space Sciences and Engineering, University of Michigan, Ann Arbor, MI
[4] Athabasca University Observatories, Athabasca University, Athabasca, AB, Canada
[5] UCLA Department of Earth Planetary and Space Sciences, Los Angeles, CA
[6] University of Newcastle, Newcastle, NSW, Australia
[7] Department of Electrical and Computer Engineering and Center for Space Physics, Boston University, Boston, MA
[8] Department of Atmospheric and Oceanic Sciences, University of California, Los Angeles, CA

submitted to the *Journal of Geophysical Research – Space Physics*

April 25, 2023

Key Words: geomagnetic disturbances, magnetic perturbation events, geomagnetically induced currents, GIC, substorms, geomagnetic storms

Key Points:

- Most large (≥6 nT/s) and extreme (≥ 20 nT/s) high latitude geomagnetic disturbances (GMDs) occurred during the declining phase of the sunspot cycle.
- Most extreme GMDs occurred during high-speed solar wind streams and often within 25 min after a substorm onset, but seldom within 5 min.
- Many extreme GMDs showed a poleward progression, consistent with the tailward retreat of the magnetotail reconnection region.

Abstract

Extreme (≥ 20 nT/s) geomagnetic disturbances (GMDs, also denoted as MPEs - magnetic perturbation events) – impulsive nighttime disturbances with time scale ~5-10 min, have sufficient amplitude to cause bursts of geomagnetically induced currents (GICs) that can damage technical infrastructure. In this study we present occurrence statistics for extreme GMD events from five stations in the MACCS and AUTUMNX magnetometer arrays in Arctic Canada at magnetic latitudes ranging from 65° to 75°. We report all large (≥ 6 nT/s) and extreme GMDs from these stations from 2011 through 2022 to analyze variations of GMD activity over a full solar cycle and compare them to those found in three earlier studies. GMD activity between 2011 and 2022 did not closely follow the sunspot cycle, but instead was lowest during its rising phase and maximum (2011-2014) and highest during the early declining phase (2015-2017). Most of these GMDs, especially the most extreme, were associated with high-speed solar wind streams (Vsw > 600 km/s) and steady solar wind pressure. All extreme GMDs occurred within 80 min after substorm onsets, but few within 5 min. Multistation data often revealed a poleward progression of GMDs, consistent with a tailward retreat of the magnetotail reconnection region. These observations indicate that extreme GIC hazard conditions can occur

for a variety of solar wind drivers and geomagnetic conditions, not only for fast-coronal mass ejection driven storms.

Plain Language Summary

1. Introduction

Large nighttime geomagnetic disturbances (GMDs) are known as magnetic perturbation events (MPEs) which are perturbations of 5-10 min duration and amplitudes of hundreds or more nT. These perturbation events are known to be causally related to geomagnetically induced currents (GICs) that can flow in long conductors such as electrical power lines, pipelines, and undersea cables (Boteler et al., 1998, Ngwira and Pulkkinen, 2019, Gannon et al., 2019). GICs are one of several phenomena included in the field of space weather that are triggered by increased solar activity that lead to dangerous levels of magnetospheric and ionospheric disturbances. Extreme GIC events that extend to middle and even low latitudes have been identified for over a century, beginning with the "Carrington event" in 1859 (Carrington, 1859, Tsurutani et al., 2003, Cliver and Dietrich, 2013) and include those related to large geomagnetic storms in May 1921 and March 1989 (Hapgood, 2019; Boteler, 2019; Love et al., 2019). Early reviews focused on the generation of GMDs during geomagnetic storms (e.g., Kappenman, 2001), but more recent studies have found that large nighttime GMDs are often more closely related to substorms, which can occur during both storm and non-storm times.

Great (low-latitude) aurorae and related extreme GIC events are associated chiefly with coronal mass ejection (CME)-driven storms and rarely with corotating interaction region (CIR)-driven storms because the aurorae do not progress as far equatorward for CIR-driven storms (Borovsky and Denton, 2006). Borovsky and Denton (2006) also noted that both CIRs and the high-speed solar wind streams that typically follow them can be drivers of storms, and that when recurring CIR-driven storms were ongoing (which tends to be in the declining phase of the solar cycle), the durations of high-speed streams were longer. Mursula et al. (2022) showed the importance of variations in the width of the heliospheric current sheet (HCS) for the relative

occurrence of geomagnetic storms related to CMEs, HSS/CIRs, and slow solar wind, respectively, such that a wide HCS made large and moderate HSS/CIR storms occur in the early declining phase in recent cycles 23 and 24 (1996-2019), while in the more active cycles 20–22 (1964-1996) they occurred in the late declining phase (their Figure 5).

Tsurutani et al. (2006) reviewed the causes, characteristics, and consequences of CIRs and high-speed streams, in particular their association with auroral substorms. Tsurutani and Gonzalez (1987) denoted the high-speed stream following the passage of a CIR past Earth as a High Intensity Long Duration Continuous AE Activity (HILDCAA) interval. HILDCAAs were originally identified during solar maximum years as intervals during which the AE index remained above 200 nT for 48 hours and that AE < 200-nT intervals were less than 2 hours in duration. However, Tsurutani et al. (1995) noted that similar extended intervals observed during the declining phase of the sunspot cycle were characterized by continuous auroral substorms stimulated by large-amplitude Alfvén waves within the high-speed streams. Tsurutani et al. (2011) concluded that the major cause of geomagnetic activity during high-speed streams is large amplitude interplanetary Alfvén waves.

There have been significant efforts worldwide to understand and forecast GICs, by developing empirical and numerical models that can predict their timing and locations (Morley, 2020). Considerable success has been achieved for predicting large-scale magnetospheric features but predicting dB/dt events with amplitude larger than 1.5 nT/s remains a challenge (Pulkkinen et al., 2013, 2017). Morley (2020) noted that while coupled frameworks and global MHD models have been shown to perform well (on average) at predicting the Dst index (Liemohn et al., 2018) and have had some success at predicting geomagnetic perturbations (Pulkkinen et al., 2013), statistical studies of simulations have shown a significant tendency to underestimate the magnitude of auroral zone magnetic perturbations (Haiducek et al., 2017; Pulkkinen et al., 2013).

More recently, Al Shidi et al. (2022) noted the Space Weather Modeling Framework (SWMF)Geospace model that is used by the NOAA Space Weather Prediction Center (SWPC) to produce ground magnetic perturbation maps has been comprehensively validated with respect to predictions of Dst and the polar cap potential (Pulkkinen et al., 2022). The Al Shidi et al.

(2022) results showed that regional predictions at mid-latitudes were also quite accurate, but that high-latitude regional disturbances were difficult to predict. Pilipenko et al. (2023) also tested this model, found that the predicted magnetic field variability dB/dt in East Scandinavia was more than an order of magnitude less than that observed, and suggested that there might be some magnetotail physics that is not captured in current global models.

Al Shidi et al. (2022) noted that the difficulty in predicting high-latitude regional disturbances reflects the tendency of this model to miss strong auroral zone latitude activity associated with substorms or other localized magnetotail processes that drive currents that couple to the ionosphere. Juusola et al.2019 (2023) noted that Pulkkinen et al. (2003) and more recently Dimmock et al. (2019) have suggested that GICs are primarily driven by small-scale spatiotemporal structures superimposed on the large-scale westward electrojet (WEJ). Weygand et al. (2021) confirmed this using a large statistical study finding that most nighttime GMDs occurred under a westward electrojet, including many within the Harang current system. Several studies have shown that nighttime GMDs were highly localized, with half-amplitude radii of a few hundred km (Ngwira et al., 2018; Engebretson et al., 2019a, b; Dimmock et al., 2020; Weygand et al., 2021).

Kwagala et al. (2020) found that the version of the SWMF model they used predicted the occurrence of low derivative threshold (0.3 nT/s) intervals in a set of stations in northern Europe at a rate very close to the frequency of occurrence in reality, but that as the threshold was increased to 1.1 and 1.5 nT/s the model diverged from the real-world rate, under-estimating at lower latitudes and sometimes overestimating at higher magnetic latitudes. The model mostly underestimated the large amplitude short-lived perturbations likely associated with localized current structures. We note that it is precisely these large amplitude, localized events that comprise a large portion of ≥ 6 nT/s nighttime GMDs.

Our earlier studies of ≥ 6 nT/s nighttime GMDs using data from Arctic Canada (Engebretson et al., 2019a,b, 2021a,b) covered only two years (2015 and 2017) and focused on latitude- and local time-dependent occurrence patterns and short-term dependencies on solar wind/IMF parameters and magnetospheric activity indices. This study documents the occurrence of these largest GMDs at auroral latitudes over a nearly complete solar cycle and

shows their frequent association with high speed solar wind streams and conditions following substorm onsets. Section 2 describes the data set and analysis methods used to identify events. Section 3 compares the solar cycle distributions of ≥ 6 nT/s GMD events, sunspots, solar wind velocity, and substorm onsets. Section 4 presents an analysis of extreme (≥ 20 nT/s) GMDs and their relation to other physical quantities and indices. Section 5 presents similarities observed in three earlier studies of multiyear GMD data sets. Section 6 discusses some of the implications of these observations, and section 7 summarizes the findings.

2. Magnetometer Data Set

Vector magnetometer data used in this multi-year study were recorded at five stations in the MACCS (Engebretson et al., 1995; Engebretson et al., 2011) and AUTUMNX (Connors et al., 2016) arrays in Eastern Arctic Canada with corrected geomagnetic latitude (MLAT) ranging from 64.7° to 75.2°, all within 20° of the 0° magnetic meridian, as detailed in Table 1 and Figure 1. The Magnetometer Array for Cusp and Cleft Studies (MACCS) began operation in 1992, and the Athabasca University Themis UCLA Magnetometer Network-Extended (AUTUMNX) began operation in late 2014. Data from both arrays were sampled at a 2 Hz cadence and are presented in local magnetic coordinates with sensor axes oriented as follows: X: magnetic north, Y: magnetic east, and Z: vertically down. Events during 2015 and 2017 from these and other neighboring stations in Arctic Canada have been used in several recent studies by Engebretson et al. (2019a, 2019b, 2021a, 2021b) and Weygand et al. (2021).

All available daily data files obtained from January 2011 through December 2022 (covering approximately one solar sunspot cycle) from each of the three MACCS stations (RBY, PGG, and CDR) and two AUTUMNX stations (SALU, KJPK) were analyzed to identify GMDs with ≥ 6 nT/s amplitude. GMD amplitude thresholds of 1 nT/s have been used in many studies (e.g., Viljanen et al., 2001) and more recently by Juusola et al. (2023). A higher threshold level for GIC hazards of 5 nT/s was identified by Molinski et al. (2000), Boteler (2001) and Woodroffe et al (2016), so the ≥ 6 nT/s events identified in this study would pose significant threats to electrical infrastructure if any were present near these sites. The GMDs in the ≥ 20 nT/s subset are comparable in amplitude to those measured during extreme GIC events at lower latitudes: nine

of them exceeded 30 nT/s, and the two largest, on March 15, 2012 and September 15, 2017, had values of 44.1 and 43.3 nT/s, comparable to the largest value cited by McManus et al. (2002) of ~2700 nT/min = ~45 nT/s recorded at the Lovo observatory (55.8° CGM latitude) near Stockholm, Sweden in July 1982 (Kappenman, 2006). We remind readers, however, that large GMDs only constitute the first (but essential) step in producing GICs that pose a threat to electrical infrastructure. The spatial arrangement and value of the underlying ground conductivity, the presence of extended conducting structures (power lines and pipelines) and their orientation relative to the driving auroral currents, and the orientation and ground connections of power grid structures such as transformers all play a role in determining the severity of the resulting GICs (Arajärvi et al., 2011; Viljanen et al., 2013; Boteler and Pirjola, 2017).

Event identification made use of a semi-automated process described in detail in Engebretson et al. (2019a). This procedure began by displaying a daily magnetogram (a 24-hour 3-axis plot of the magnetic field at a given station) on a computer screen. Once a rapid (< 20 min duration) and large amplitude (> ~ 200 nT) magnetic perturbation was visually identified, the IDL cursor function was used to select times ~15 to 60 min before and after the perturbation to zoom in on the relatively short duration of the event and separate it from the times of other possible activity. After application of a 10-point boxcar mean smoothing to reduce noise and eliminate isolated non-physical spikes, the data were numerically differentiated using the 3-point Lagrangian approximation. The times and values of extrema of B and dB/dt for all three component in this interval were recorded for completeness, as also did Milan et al. (2023), and plots of the time series of data and derivatives were produced and saved. If more than one interval with a ≥ 6 nT/s derivative in one or more components was identified on a given day, this process was repeated as necessary. The minimum length of each interval was chosen to be ~5 min, so multiple peak derivatives ≥ 6 nT/s occurring within a given ~5 min interval were not counted separately. A subset of 72 events with a ≥ 20 nT/s derivative in one or more components was identified from this data set.

3. Yearly Distribution of >6 nT/s GMDs, Sunspots, Solar Wind Velocity, and Substorm Onsets

Table 2 summarizes the data set used in this study. Although the magnetometer and recording instrumentation at all MACCS stations were set up to record continuously from 2011 through 2022, and at all AUTUMNX stations from late 2013 through 2022, power outages, cut cables, and instrument malfunctions at these remote sites often resulted in no data or erroneous data at individual stations. We thus show in this table the number of available valid station days per year and the total number of ≥ 6 nT/s and ≥ 20 nT/s GMD events and the percent ratio of these events per available station day.

Figure 2a shows the occurrence percentages of ≥ 6 nT/s GMDs from each of the five stations from 2011 through 2022. Note that the traces for AUTUMNX stations SALU and KJPK began in 2014, and there were no data from SALU during 2020 or from RBY during 2011. The overall trend at each station is similar, and from 2016 through 2022 there is a clear pattern in magnetic latitude: percentages are lowest at the highest MLAT station, RBY, and at the lowest MLAT station, KJPK, and are higher and generally similar at the three stations at latitudes between these extremes. We note that the yearly nT/s/day occurrence rates shown in Table 2 are averages over all five stations, so they fall between the extremes shown in Figure 2a for individual stations.

Figure 2b shows the monthly sunspot number, obtained from the Solar Influences Data Center, (https://sidc.be/silso/datafiles/), from January 2011 through December 2022. The rising phase and maximum of sunspot cycle 24 (2011-2014) coincided with low occurrence percentages of GMDs, whereas the declining phase (2015-2017) coincided with high GMD occurrence percentages. The late declining phase and sunspot minimum (2018-2020) coincided again with decreasing GMD occurrence percentages. The early rising phase of Cycle 25 coincided with rising GMD occurrence percentages; GMD occurrence percentages in 2022 were considerably larger than those 11 years earlier (2011) at the same stations, PGG and CDR.

Figure 2c shows yearly medians and 25^{th} and 75^{th} percentile values of the solar wind velocity (Vsw), based on 1-hour averages obtained from the OMNI database via CDAWEB (https://cdaweb.gsfc.nasa.gov/) for these same years. The highest yearly median and especially 75^{th} percentile velocities coincided in time with the largest GMD occurrence percentages (2015-2017) and the lowest yearly velocities (2013-2014 and 2020) coincided approximately with the

smallest GMD occurrence percentages (2012-2014 and 2020). The fractional range in GMD occurrences (a factor of ~3) was much larger than the fractional range of Vsw values. We note especially that the 75th percentile values were further from the median than the 25th percentile values during 2015-2017 and 2019, indicating a more extended high-velocity tail of the Vsw distributions during those years.

Figure 2d, which shows the yearly number of substorms in the Newell and Gjerloev (2011a, 2011b) substorm list obtained from SuperMAG (https://supermag.jhuapl.edu/substorms/), reveals a temporal pattern with variations similar to those of the Vsw medians (Figure 2c). (Note that as of April 12, 2023 no substorm list was available for year 2022.) Consistent with this pattern, the multiyear statistical study by Borovsky and Yakymenko (2017) found that substorm occurrence rates were substantially higher during the declining phase of the solar cycle than they are during the other three phases of the solar cycle, and in particular that the substorm occurrence rate was greatly increased when high-speed solar wind impacted Earth (their Table 3). They also concluded that the average level of driving of the magnetosphere was highest under these conditions.

The close connection shown here between the occurrence of large GMDs and increased Vsw is also evident in Figures S3 and S4 of the supporting information for the superposed epoch study of Engebretson et al. (2021b). Figure S3 in that study showed that the medians of Vsw were relatively constant from 4 hours before to 4 hours after GMD occurrences, for both premidnight and postmidnight events and for three ranges of time delays between substorm onset and GMD occurrence, but with somewhat more variability as the number of events per station decreased from 151 down to 6. Figure S4 showed two example plots of the 8-hour Vsw traces during all the premidnight events at two representative stations, CDR and KJPK, that occurred between 0 and 30 minutes after the most recent substorm onset. In both plots the number of events with Vsw values above 550 km/s exceeded those below 500 km/s. Most of the individual traces shown were rather flat over the 8-h interval and revealed no consistent temporal pattern.

Engebretson et al. (2021b) also investigated the dependence of GMD occurrences on the solar wind dynamic pressure (Psw). Figure 4 of that paper again showed that the mean Psw

traces from 4 hours before to 4 hours after GMD occurrences were relatively constant for all categories except for those with 7 or fewer events. In the case of Psw, however, in nearly every category shown in Figure 4 at least one Psw trace had values exceeding 10 nPa. Figure 5 of that paper showed two such examples, corresponding to panels a2 and a5 of Figure 4.

4. Analysis of ≥ 20 nT/s GMDs

Figure 3 shows a comparison of the occurrence percentages of ≥ 6 nT/s GMDs at each of the five stations (panel a, repeated from Figure 2) to the occurrence percentage for each year of the sum of events at all five stations divided by the sum of the available station days for both ≥ 6 nT/s GMDs and ≥ 20 nT/s GMDs (panel b). Both traces followed roughly the Vsw and substorm trends shown in Figure 2, but the variation in the ≥ 20 nT/s GMD trace was much larger. The ratio of the ≥ 6 nT/s trace to the ≥ 20 nT/s was between 40 and 50 during 2015-2017, but was between 75 and 80 during 2018 and 2019, and was above 100 in 2020 and 2021.

Figure 4a shows a histogram of the hourly averaged solar wind velocity (Vsw) observed during each of the ≥ 20 nT/s GMD events, and Table 3 shows the distribution of these events as a function of both year and Vsw. Figure 4b shows the distribution of all Vsw values at 1 min resolution over these same years. None of the ≥ 20 nT/s GMDs occurred when Vsw < 350 km/s; most occurred in association with the high-velocity tail of this distribution, which is well fit by a decreasing exponential. Table 3 indicates that the ≥ 20 nT/s GMDs with Vsw values above 600 km/s occurred mostly between 2015 and 2017.

Of the five ≥ 20 nT/s events with Vsw < 400, two occurred during the first day of recovery after an intense CME storm, one occurred during the main phase of a modest CME storm, and one during a strong sudden impulse event before a CME storm. The fifth event, at 0349 UT December 7, 2018, also appeared with ≥ 6 nT/s amplitude at three of the other four stations. It occurred during quiet conditions according to the OMNI time-shifted data base, but data from Themis D, inbound near 10 MLT from the solar wind toward the magnetopause, observed a sharp outward motion of the bow shock simultaneous with a ~20 nT negative jump in the IMF at 0358 UT (not shown) that may have stimulated this GMD event. The Yermolaev storm list (described below) identified this event as an interplanetary shock.

Many studies of intense or extreme dayside GMDs have noted a correlation between their occurrence and rapid increases in solar wind pressure (Psw), such as are often characteristic of sudden impulses or sudden commencements (e.g., Le et al., 1993; Carter et al., 2015; Oliveira et al., 2018). Table 4 shows the distribution of ≥ 20 nT/s GMDs as a function of year, Vsw below and above 500 km/s, and the presence or absence of rapid Psw increases of 1.5 nT or more from 2011 through 2022. Of these extreme GMDs, rapidly rising Psw values were associated with 38% of those that occurred when Vsw < 500 km/s, but with only 24% of the much larger number of events when Vsw > 500 km/s. Therefore, the majority of events for both ranges of Vsw occurred during relatively steady Psw conditions.

The ≥ 20 nT/s GMD events were also sorted as functions of geomagnetic storm conditions and phase in two complementary ways. In Table 5 they are sorted into four magnetic storm categories including main through late recovery phases, SI/SC events, and quiet intervals. The extreme GMDs occurred most often during the main, early, and late recovery phases of moderate geomagnetic storms, weak geomagnetic storms, and quiet intervals, in that order.

Table 6 shows the ≥ 20 nT/s GMD distribution based on the Yermolaev et al. (2009) list of types of solar wind as applied to the 5-min resolution OMNI data base, http://www.iki.rssi.ru/pub/omni/catalog/. All available time intervals were identified as either FAST (V > 450 km/s) or SLOW (V < 450 km/s) solar wind, and further identified, when appropriate, as forward interplanetary shocks (IS), corotating interaction regions (CIRs), and three subcategories of CMEs: ejecta, magnetic clouds, and sheath compression regions before fast ejecta or magnetic clouds. Other types listed but not represented in this data set were heliospheric current sheets, reverse interplanetary shocks, and intervals of rarefied plasma. In Table 6 we have grouped the events into seven categories: interplanetary shocks, CMEs and CIRs with slow or fast solar wind, and fast or slow solar wind not associated with either a CME or CIR. No events occurred during slow solar wind conditions not associated with either a CME or CIR. This table shows that 38 of the 72 GMDs occurred during fast solar wind conditions not

during passages of CMEs or CIRs, and another 25 occurred during fast solar wind conditions during CMEs or CIRs. Only 7 events occurred during intervals when Vsw < 450 km/s.

The frequent association of these GMDs with geomagnetic storms might suggest that they most often occurred during disturbed magnetospheric conditions, but analysis of their distribution as a function of SYM/H (Table 7) indicates otherwise. Only 16 of the 72 ≥ 20 nT/s GMDs events occurred when SYM/H was ≤ -51 nT. Most of these GMDs instead occurred when SYM/H was -50 nT or higher during conditions associated with weak magnetic storms or quiet conditions. The concentration of events when SYM/H was above -40 nT was strongest during 2016 and 2017, when eight out of 11 and 14 out of 18 ≥ 20 nT/s GMDs, respectively, occurred. The patterns for 2015 and 2017 can be compared with Figure 5 of Engebretson et al. (2021a), which showed that ≥ 6 nT/s GMDs were also most likely to occur for SYM/H values between -40 and 0 nT. We remind readers, however, that during more intense storms the auroral oval moves much farther equatorward, out of the primary range of auroral zone magnetometers.

Figure 5 shows the temporal relation of ≥ 20 nT/s GMD events to substorm onsets. The number of events decreased gradually with increasing time delays, but with no maximum at the time of onset or during the first 10 min. This figure can be compared with Figure 2 of Engebretson et al. (2021a), which showed scatter plots of the amplitude of all ≥ 6 nT/s GMD events at five Canadian Arctic stations (the same stations except that Iqaluit was included rather than Pangnirtung) as functions of their delay after the most recent substorm onset, from 0 to 120 min. Figure 2 of Engebretson et al. (2021a) also showed that the number of events decreased gradually with increasing time delays at each station, with no maximum at the time of onset or during the first 10 min, consistent with the trends shown in Figure 5.

A majority of the most extreme (≥ 20 nT/s) GMD events were also associated with higher-frequency, transient-large amplitude dB/dt intervals (TLAs) occurring prior to or within GMDs (McCuen et al., 2021). It has been recently shown in McCuen et al. (2023) that these TLA signatures were exclusive to the auroral zone in the high magnetic latitude region. TLA events showed a very similar relation to substorm onsets as GMDs, i.e., decreasing number of events with longer delay from substorm onset, but with no maximum at the time of onset.

The lack of a close temporal association between nighttime GMDs and substorm onsets has been evident in some earlier detailed studies as well. Ngwira et al. (2018) showed observations of a geomagnetic storm on March 17, 2015 during which strong dB/dt events appeared from 7 to 12 min after a substorm onset, and Engebretson et al. (2019b) showed that on November 11, 2015 there was a ~10 min delay between substorm onset and the appearance of GMDs. This delay was also noted by Juusola et al. (2023) in a study of five GMD events that were responsible for the most intense derivative magnitudes in external sources (due to ionospheric and magnetospheric electric currents) observed by the IMAGE array in Scandinavia between 1994 and 2018. They found that there were no substorm onsets or sudden intensifications of the WEJ among them. They concluded that although the intensifying westward electrojet after substorm onset may be a typical source of moderate derivative values (as shown in Figure 3 of Viljanen et al. 2006 for ≥ 1 nT/s events), the rarer events with much larger derivatives tended to occur during later times.

Figure 6 shows the distribution of ≥ 20 nT/s GMD events in magnetic local time. The occurrences are dominated by a "premidnight" population from 17 MLT to near local midnight and a smaller "postmidnight" population from near local midnight to 06 MLT. The distribution is very similar to that of the much larger set of ≥ 6 nT/s GMD events in this region shown in Figure 4 of Engebretson et al. (2021a). It is notable that no ≥ 20 nT/s GMD events occurred between 06 and 17 MLT. These distributions are consistent with the observations of Schillings et al. (2022), who identified two "hot spots" of > ±500 nT/min dB/dt spikes in the premidnight and morning magnetic local time sectors, using 1- minute cadence data from all available stations worldwide in the SuperMAG database during all magnetic storms from 1980 through 2020, independently of the geographic latitude and longitude of a given station.

Figure 7 shows the monthly variation of large GMD occurrences. Panel a shows the average number of events per month from 2011 through 2021 (no year 2022 substorm list was available on SuperMAG as of 4/12/2023). Panel b shows the monthly average number of ≥ 6 nT/s GMDs after taking into account the less than complete magnetometer data coverage during several years at individual stations, and panel c shows the distribution of ≥ 20 nT/s GMDs from 2011 through 2022. The levels for SALU and KJPK are elevated compared to those

373 at the other stations because no data were available from these two stations from 2011
374 through 2013, years with low numbers of GMDs at the other stations, as shown in Figure 2a.
375 The well-known semiannual variation in substorms appears to hold approximately for GMDs as
376 well (panels b and c), consistent with the frequent occurrence of GMDs after substorms.
377 The association between GMDs and substorm occurrences was not consistent over the
378 solar cycle. Figure 8 shows that the yearly ratio of ≥ 6 nT/s GMDs to substorms was lowest
379 during the first years of sunspot Cycle 24 (between 2011 and 2014) but was higher in later
380 years. This trend may reflect the fact that more intense substorms are associated with higher
381 speed solar wind streams. Longer-term data from other stations or arrays may be useful for
382 checking whether this pattern holds for previous sunspot cycles.
383 Table 1 shows that the separation between nearest stations in this study ranged in the
384 north-south direction from 227 km (CDR –SALU) to 776 km (SALU – KJPK) but were nearly equal
385 in the east-west direction: 513 km (RBY-CDR) and 546 km (CDR-PGG). Of the 72 ≥ 20 nT/s
386 events, 43 (60%) were accompanied within 10 minutes (and often less) by events with
387 amplitude ≥ 6 nT/s at one or more of the other stations in this data set. Our five-station data
388 set includes the amplitude and time of extrema (+ and -) in all three components of the
389 derivative at each station. We identified a probable spatial GMD progression if there was a
390 consistent time difference in at least five of these six component extrema. Using this criterion,
391 we identified 25 GMDs as progressing primarily northward (poleward) and one primarily
392 westward. The remaining 17 events were stationary or unclear. In many of these latter cases
393 large GMDs appeared only at the nearest pair of stations, CDR and SALU. The Vsw distributions
394 of the northward, stationary, and unclear events were similar, indicating that Vsw had little or
395 no influence regarding this spatial progression. Three similar multi-station events observed
396 during 2015 were presented by Engebretson et al. (2019b) using stacked magnetograms,
397 spherical elementary current systems (SECS) maps (Weygand et al., 2011) and images from a
398 set of all-sky imagers. Two of the three showed a poleward progression. Ngwira et al. (2018)
399 presented observations of GMDs by multiple magnetometers during two geomagnetic storms
400 that also showed a clear poleward progression, and McCuen et al. (2023) presented a more
401 complex event in 2016 during which separate regions of GMDs, currents, and auroras over the

west and east coasts of Hudson Bay both showed a poleward progression. We discuss possible mechanisms causing these poleward progressions below.

5. Comparison to Three Other Studies of Multiyear GMD Data Sets

We are aware of three other studies of GMDs that span one or more recent solar cycles. Milan et al. (2023) presented a comprehensive survey of >300 nT perturbations in any component of the magnetic fields in 1 min cadence data from all available magnetometer stations above 50° magnetic latitude in the SuperMAG data base from 1995 to 2020. Kellinsalmi et al. (2022) compiled the distribution of >1 nT/s GMDs observed at Sodankylä, Finland from 1996 through 2018, and Marshall et al. (2011) presented GMD activity index data from 1985 through 2009 from several sites across Australia. The solar cycle occurrence patterns observed by these studies, with maxima during the declining phase, were all similar to those presented here.

Milan et al. (2023) cataloged all instances of minute-to-minute changes in magnetic field components ("spikes") that exceeded 300 nT, which corresponds to a derivative threshold of 5 nT/s. Although several earlier studies (e.g., Viljanen, 1997; Viljanen et al., 2006; Engebretson et al., 2019a, 2021b) reported a lack of good correlation between ΔB and dB/dt amplitudes during large MPEs, these perturbations remain a useful proxy for GMDs, especially when higher time resolution data are not available. Milan et al. (2023) identified two local time regions of greatest activity: premidnight (17-02 MLT) and postmidnight (02-09 MLT), consistent with the observations of Engebretson et al. (2021a) and Schillings et al. (2022). They noted maximum occurrence rates during the declining phases of both Solar Cycles 23 and 24, and their Figure 3 showed similar occurrence trends in spikes and high-speed streams. Based on a comparison of yearly spike occurrences in Figure 3a that showed similar patterns using thresholds of 100, 200, 300, and 400 nT/min, Milan et al. (2023) suggested that their shapes did not depend on the magnitude of the spikes. However, although the timing of these patterns did not change, the ratio of maxima to minima using these different thresholds increased from the > 100 nT/min trace to the > 400 nT/min trace. We observed a similar trend in data presented in Table 2 and Figure 3b above for ≥ 6 nT/s and ≥ 20 nT/s events; the temporal patterns were again similar,

431 but the amplitude of their variations increased with increasing thresholds, even for extreme
432 GMDs.

433 Kellinsalmi et al. (2022) included the yearly totals of > 1 nT/s GMDs recorded at
434 Sodankylä, Finland (63.9° MLAT) in their Figure 7. A comparison of panels a and b of Figure 9
435 here shows that the trend in the yearly total of these > 1 nT/s GMDs was similar to that in
436 sunspots between 1996 and 2001 (the rising part of sunspot Cycle 23), and during the sunspot
437 minimum years and early part of Cycle 24, between 2006 and 2012. However, the sharp peak
438 in GMDs during 2003 matched well with sharp peaks in Vsw (panel c) and substorms (panel d),
439 while there was no corresponding peak in sunspots (panel b). Subsidiary peaks in GMDs in
440 2005 and 2017 also matched those in Vsw and substorms but not sunspots, and the relative
441 minima in GMDs during 2001 and 2002 matched similar minima in Vsw and substorms rather
442 than the simultaneous rise in sunspots. We note that the 75th percentile values were further
443 from the median than the 25th percentile values during 2003 and 2005-2008, again indicating a
444 more extended high-velocity tail of the Vsw distributions during those years, but that there
445 were fewer substorms and also fewer GMDs during 2006-2008. As noted above, the lower
446 GMD threshold of > 1 nT/s allows the inclusion of many substorm onsets in the GMD count, so
447 the drop in GMD activity during these three years may primarily reflect the drop in substorms.

448 An earlier study by Marshall et al. (2011) also showed similarities to the patterns
449 presented above at lower latitudes, ranging from -22.7° to -50.7° magnetic latitude, from 1985
450 through 2009. Figure 10a, a copy of Figure 7 of Marshall et al. (2011), shows the values of their
451 GICy index, a frequency domain filter applied to geomagnetic field data recorded at seven
452 stations across Australia to determine GIC risk level thresholds. The highest latitude station,
453 Hobart, Tasmania, only had data available for the second solar cycle. The horizontal yellow,
454 orange, and red lines are the lower limit thresholds for the “low,” “moderate,” and “high”
455 threat levels defined in that study. The red dots in Figure 10a show GICy index values for every
456 event exceeding the threshold for “low” risk, and also shows the sunspot number during these
457 same years. Figure 10b shows the yearly Vsw averages and percentiles, and Figure 10c shows
458 the yearly number of substorms, again from the SuperMAG list.

During 1989 (the end of the rising phase of the solar cycle) and 1991 (the beginning of the declining phase) GMDs with GICy values > 50 occurred when all three of sunspot numbers, yearly Vsw averages, and yearly substorm averages had relative maxima. The two index values near 100 in 1989, reaching the moderate risk level, occurred during the 13 March 1989 superstorm. We note that the 75th percentile value of Vsw during 1991 was comparable to those during the declining phase of Cycle 23, again indicating a longer high velocity tail.

Only one GICy ~ 50 event (just above the low-risk threshold) occurred during the rising phase of the next sunspot cycle (from 1997 through 2000), but a large number of events occurred during the declining phase (from late 2000 through 2006). Most of these events were observed at Hobart, including 21 events over nine different days in the moderate risk range.

We also note that although the peaks of Vsw and substorms were both highest in 1994 and 2003, no GMDs were observed at Australian stations during 1994, and the number of GMD events between late 2000 and the end of 2006 was high, their yearly variations did not follow closely the variations in Vsw or substorms. The lack of correlation with substorm onsets may be due to the location of these stations far from the auroral zone, but the lack of correlation with increased levels of Vsw does not necessarily follow from this observation. This data set thus shows both the strong dependence of GMDs on the phase of the sunspot cycle (most clearly seen at the mid- latitude (Hobart station) and the probable multiplicity of driving factors that may govern their occurrence in regions equatorward of the auroral zone.

6. Discussion

We have noted above not only the strong connection between intense GMDs and high speed solar wind streams, as has been found in several other studies, but the frequent poleward progression of these GMDs. We here review recent studies that may indicate the physical connection between these two phenomena.

Tsurutani and Gonzalez (1987) and Tsurutani et al. (2011) concluded that the major cause of geomagnetic activity during extended HILDCAA intervals, associated with high speed solar wind streams, is large amplitude Alfvén waves. Dai et al. (2023) confirmed these findings in multiple events in corotating interaction region-driven geomagnetic storms. They noted that

Alfvénic fluctuations in the solar wind associated with repetitive substorms contributed to the extended recovery phases of geomagnetic storms, and that such intervals were promptly followed by hundreds of nT increases in the AE and AU auroral electrojet indices within 10–20 minutes. Dai et al. (2023) also presented a phenomenological model of strongly driven substorms, in which the increase of the AE index is linked to dayside reconnection mainly through the ionosphere (through enhanced two-cell convection) instead of the magnetotail, and suggested that this pattern is expected to be particularly viable and even dominant in the descending phase of the solar cycle.

Earlier studies by Kim et al. (2009) and Lyons et al. (2009) also found evidence for links between dayside reconnection and nightside disturbances via increased ionospheric convection. Kim et al. (2009) noted that north-south solar wind fluctuations enhanced ionospheric convection flows in the dayside polar cap and that ULF power in the solar wind enhanced the convection strength, independent of an observed direct effect from the solar wind speed. They also noted that these large oscillations of convection flow speeds occurred independent of the direction of the IMF, found correlations with Vsw and Psw, and presented evidence that the power in the IMF fluctuations affects the convection independently of effects of Psw fluctuations. Lyons et al. (2009) found that there were also close relationships between solar wind fluctuations and convection flows in the nightside ionosphere and within the plasma sheet, indicating that the effect of the solar wind fluctuations was global.

Lyons et al. (2011, 2013) extended this connection to auroral poleward expansions, post-onset auroral streamers, and the duration of post-onset auroral activity. Lyons et al. (2013) noted that the more abrupt and larger magnetic field responses came not from auroral onsets but in association with post-onset streamers at times varying from just a few minutes to well over 30 min after substorm auroral onset if there was a prolonged period of streamers. Similarly, Nishimura et al. (2013) presented evidence indicating that plasma transport (observed as airglow patches) originating from the dayside and reaching the nightside open-closed boundary may trigger plasma sheet flow bursts and play a crucial role in both pre- and post-onset auroral activity.

The poleward progression of these GMDs and associated increases in ionospheric and field-aligned currents are related to the tailward retreat of the magnetotail reconnection region, as suggested in observational studies by Nakamura et al. (2011) and Ieda et al. (2016). The reconnection region associated with a substorm onset may initially be close to Earth, but as the magnetic field dipolarizes, subsequent auroral breakups correspond to reconnection regions farther downtail. This tailward retreat corresponds to the poleward shift of the magnetic footprint.

A recent study by Zou et al. (2022) used coordinated observations from THEMIS and Geophysical Institute Magnetometer Array magnetometers and THEMIS all-sky imagers to statistically examine large dB⁄dt intervals during geomagnetic storms from 2015 to 2016. They identified a variety of auroral drivers, including poleward expanding auroral bulges, auroral streamers, poleward boundary intensifications, omega bands, and pulsating auroras. In particular, they noted that poleward expanding auroral bulges drive large dB/dt events that spread progressively poleward, and periodic injections of streamers drive large dB/dt events that occurred in periodic bursts.

Although the importance of the auroral drivers for GMDs suggested by Zou et al. (2022) is consistent with this study and our previous studies, we have found that these auroral drivers are not limited to the occurrences of geomagnetic storms. Instead, the most intense nighttime GMDs at high latitudes and extending toward midlatitudes are related statistically to substorms and especially extended periods of magnetotail activity related to high speed streams. Two of the three events presented by Engebretson et al. (2019b) noted the association between intense GMDs and auroral streamers, as did one event shown in Figure 11 of Weygand et al. (2021).

7. Summary and Conclusions

This study has presented observations of ≥ 6 nT/s and ≥ 20 nT/s GMD occurrences at high latitudes (nearly all of them during local nighttime) during the most recent sunspot cycle and compared them to several parameters that are expected to be associated with them: a measure of solar activity (monthly sunspot numbers), measures of the interaction between the

545 solar wind and the magnetosphere (the solar wind velocity Vsw and dynamic pressure Psw), a
546 measure of activity in the magnetotail (the number of substorm onsets), and a measure of
547 magnetic storm intensity (the SYM/H index). Our previous studies have shown a strong short-
548 term relation between the occurrence of ≥ 6 nT/s GMDs and prior ~30 min intervals of
549 southward IMF Bz, which is also related to magnetotail activity and the occurrence of substorm
550 onsets.

551 1. In the data sets presented here, GMDs ≥ 6 nT/s occurred more often during the
552 declining phase of sunspot cycles, rather than during their first half or during years of sunspot
553 maxima or minima. This was evident in GMDs observed in Arctic Canada between 2011 and
554 2022 (this study) and was consistent in large part with three published studies using data
555 covering multiple years. It is notable that even at mid- and low latitudes, many more GMDs
556 occurred during the declining phase of the sunspot cycle.

557 2. The yearly GMD occurrence percentages in this study agreed better with yearly
558 values of the solar wind velocity, and only slightly less well with yearly average values of
559 substorm occurrences. Many or most of these GMDs were associated with high-speed solar
560 wind streams that can occur either in association with geomagnetic storms stimulated by high-
561 speed CMEs or CIRs or during their extended aftermath, during HILDCAA intervals.

562 3. Occurrences of ≥ 20 nT/s GMDs in this study were more strongly associated with the
563 declining phase of the sunspot cycle and with high Vsw values than ≥ 6 nT/s GMDs. Occurrences
564 of ≥ 20 nT/s GMDs were most common within 25 min after a substorm onset (but few occurred
565 within 5 min), and all occurred within 80 min after an onset. These timing patterns appeared
566 also in our earlier studies of ≥ 6 nT/s GMDs. Occurrences of these GMDs showed a peak in the
567 SYM/H range from -40 to -11, i.e., mostly during modestly or weakly disturbed geomagnetic
568 conditions, but as noted above, during more intense magnetic storms the auroral oval moves
569 much farther equatorward, so large GMDs would tend to not be as often observed at high
570 latitudes.

571 4. Of the 43 of 72 ≥ 20 nT/s GMD events that were also observed with large amplitude
572 at neighboring stations, 25 showed a poleward progression, one a westward progression, 17
573 were stationary or unclear, and none were equatorward. The mechanisms governing this

poleward progression may be related to auroral poleward expansion, which may be attributed to the tailward retreat of the magnetotail reconnection region, which is now known to occur during times of roughly continuous disturbed conditions stimulated by high speed solar wind streams and their associated Alfvén waves.

The combination of the strong connection between intense and extreme GMD events at high latitudes and both high speed solar wind streams and intervals following substorm onsets, rather than with intense magnetic storms and large negative SYM/H values, as well as the relative absence of such events during the rising phase of the last three solar cycles, suggests that warnings of intense GMDs should not be restricted to the rising phase of the sunspot cycle or times when CMEs are approaching Earth. Rather, the relatively less studied occurrence of high-speed solar wind streams and HILDCAA activity that are associated with geomagnetically disturbed conditions during the declining phase of the sunspot cycle may provide additional clues as to the proximate causes of these often impulsive nighttime disturbances.

Acknowledgments

We thank David Boteler for helpful discussions. This research was supported by National Science Foundation grants AGS-2013648 to Augsburg University and AGS-2013433 to the University of Michigan. Martin G. Connors thanks NSERC for research support and the Canadian Space Agency for support of AUTUMNX. Work by James M. Weygand was supported by NASA grants HSR-80NSSC18K1227 and SWO2R 80NSSC20K1364, NASA contract HPDE-80GSFC17C0018, NSF grant GEO-NERC 2027190, and NSF grant AGS-2013648 via subcontract from Augsburg University. Work by Larry R. Lyons was supported by NSF grants AGS-20191955 and AGS-2055192 and NASA grants 80NSSC20K1314 and 80NSSC22K0749. Work by Yukitoshi Nishimura was supported by NASA grants 80NSSC18K0657, 80NSSC20K0604, 80NSSC20K0725, 80NSSC21K1321, 80NSSC22K0323, and 80NSSC22M0104, NSF grants AGS-1907698 and AGS-2100975, and AFOSR grant FA9559-16-1-0364. THEMIS is supported by NASA NAS5-02099 and the Canadian Space Agency.

Author Contributions

Conceptualization: Mark J. Engebretson

Data curation: Erik S. Steinmetz, Brett A. McCuen, Martin G. Connors

Formal analysis: Mark J. Engebretson

Funding acquisition: Mark J. Engebretson

Investigation: Mark J. Engebretson, Lily Yang, Vyacheslav A. Pilipenko, Mark B. Moldwin, Brett A. McCuen, Martin G. Connors, James M. Weygand, Yukitoshi Nishimura, Larry R. Lyons, Colin L. Waters, Christopher T. Russell

Methodology: Mark J. Engebretson, James M. Weygand

Data Availability Statement

MACCS magnetometer data are available in IAGA 2002 ASCII format at http://space.augsburg.edu/maccs/requestdatafile.jsp and AUTUMNX magnetometer data are available in IAGA 2002 ASCII format at http://autumn.athabascau.ca/autumnxquery2.php?year=2015&mon=01&day=01. GMD data from the five stations used in this study are available at the University of Michigan's Deep Blue Data Repository at https://doi.org/10.7302/275e-da06. The SuperMAG substorm database is available at http://supermag.jhuapl.edu/substorms/. Jesper Gjerloev is SuperMAG Principal Investigator. . The Yermolaev storm list and related documentation are available at http://www.iki.rssi.ru/pub/omni/catalog/.

References

Al Shidi, Q., Pulkkinen, T., Toth, G., Brenner, A., Zou, S., & Gjerloev, J. (2022). A large simulation set of geomagnetic storms—Can simulations predict ground magnetometer station observations of magnetic field perturbations? Space Weather, 20, e2022SW003049. https://doi.org/10.1029/2022SW003049

630 Arajärvi, E., Pirjola, R. J., & Viljanen, A. (2011), Effects of neutral point reactors and series
631 capacitors on geomagnetically induced currents in a high-voltage electric power transmission
632 system. *Space Weather*, *9*, S11005. https://doi.org/10.1029/2011SW000715
633
634 Borovsky, J. E., & Denton, M. H. (2006). Differences between CME-driven storms and CIR-driven
635 storms. *Journal of Geophysical Research*, *111*, A07S08. https://doi.org/10.1029/2005JA011447
636
637 Borovsky, J. E., and Yakymenko, K. (2017). Substorm occurrence rates, substorm recurrence
638 times, and solar wind structure. *Journal of Geophysical Research: Space Physics, 122,* 2973-
639 2998, doi:10.1002/2016JA023625
640
641 Boteler, D. H. (2001). Assessment of geomagnetic hazard to power systems in Canada. *Natural*
642 *Hazards*, *23*, 101–120. https://doi.org/10.1023/A:1011194414259
643
644 Boteler, D. H. (2019). A 21st century view of the March 1989 magnetic storm. *Space Weather*,
645 *17*, 1427–1441. https://doi.org/10.1029/2019SW002278
646
647 Boteler, D. H., Pirjola, R. J., & Nevanlinna, H. (1998). The effects of geomagnetic disturbances on
648 electrical systems at the Earth's surface. *Advances in Space Research*, *22*, 17–27.
649 https://doi.org/10.1016/S0273-1177(97)01096-X
650
651 Boteler, D. H., & Pirjola, R. J. (2017). Modeling geomagnetically induced currents. *Space*
652 *Weather*, 15, 258– 276. https://doi.org/10.1002/2016SW001499
653
654 Carrington, R. C. (1859). Description of a Singular Appearance seen in the Sun on September
655 1, 1859. *Mon. Not. Roy. Astron. Soc., 20,* 13–15. http://dx.doi.org/10.1093/mnras/20.1.13
656
657 Carter, B. A., Yizengaw, E., Pradipta, R., Halford, A. J., Norman, R., & Zhang, K. (2015).
658 Interplanetary shocks and the resulting geomagnetically induced currents at the equator.

659 *Geophysical Research Letters, 42*, 6554–6559. https:/doi.org/10.1002/2015GL65060
660
661 Chapman, S. C., Horne, R. B., & Watkins, N. W. (2020). Using the aa index over the last 14 solar
662 cycles to characterize extreme geomagnetic activity. *Geophysical Research Letters, 47(3),*
663 e2019GL086524. https://doi.org/10.1029/2019GL086524
664
665 Cliver, E. W., & Dietrich, W. F. (2013). The 1859 space weather event revisited: Limits of
666 extreme activity. *Journal of Space Weather and Space Climate*, *3*, 31.
667 https://doi.org/10.1051/swsc/2013053
668
669 Connors, M., Schofield, I., Reiter, K., Chi, P. J., Rowe, K. M., & Russell, C. T. (2016). The
670 AUTUMNX magnetometer meridian chain in Québec, Canada. *Earth, Planets and Space*, *68*(1).
671 https://doi.org/10.1186/s40623-015-0354-4
672
673 Dai, L., Han, Y., Wang, C., Yao, S., Gonzalez, W. D., Duan, S., Lavraud, B., Ren, Y., & Guo, Z.
674 (2023). Geoeffectiveness of Interplanetary Alfvén Waves, I, Magnetopause Magnetic
675 Reconnection and Directly Driven Substorms. *The Astrophysical Journal, 945:47*.
676 https://doi.org/10.3847/1538-4357/acb267
677
678 Dimmock, A. P., Rosenqvist, L., Welling, D. T., Viljanen, A., Honkonen, I., Boynton, R. J., and
679 Yordanova, E. (2020). On the regional variability of dB=dt and its significance to GIC, *Space*
680 *Weather, 18,* e2020SW002497. https://doi.org/10.1029/2020SW002497
681
682 Engebretson, M. J., W. J. Hughes, J. L. Alford, E. Zesta, L. J. Cahill, Jr., R. L. Arnoldy, and G. D.
683 Reeves (1995). Magnetometer array for cusp and cleft studies observations of the spatial
684 extent of broadband ULF magnetic pulsations at cusp/cleft latitudes. *Journal of Geophysical*
685 *Research, 100*, 19371-19386. doi:10.1029/95JA00768
686

687 Engebretson, M., Steinmetz, E., &, , and Moldwin, M. (2011). MACCS 0.5 s Ground
688 Magnetometer Data [Data set]. Augsburg University. https://doi.org/10.48322/sydj-ab90
689
690 Engebretson, M. J., Pilipenko, V. A., Ahmed, L. Y., Posch, J. L., Steinmetz, E. S., Moldwin, M. B.,
691 Connors, M. G., Weygand, J. M., Mann, I. R., Boteler, D. H., Russell, C. T., & Vorobev, A. V.
692 (2019a). Nighttime magnetic perturbation events observed in Arctic Canada: 1. Survey and
693 statistical analysis. *Journal of Geophysical Research: Space Physics*, *124,* 7442-7458.
694 https://doi.org/10.1029/2019JA026794
695
696 Engebretson, M. J., Steinmetz, E. S., Posch, J. L., Pilipenko, V. A., Moldwin, M. B., Connors, M.
697 G., Boteler, D. H., Mann, I. R., Hartinger, M. D., Weygand, J. M., Lyons, L. R., Nishimura, Y.,
698 Singer, H. J., Ohtani, S., Russell, C. T., Fazakerley, A., & Kistler, L. M. (2019b). Nighttime
699 magnetic perturbation events observed in Arctic Canada: 2. Multiple-instrument observations.
700 *Journal of Geophysical Research: Space Physics*, *124,* 7459-7476.
701 https://doi.org/10.1029/2019JA026797
702
703 Engebretson, M. J., Pilipenko, V. A., Steinmetz, E. S., Moldwin, M B., Connors, M. G., Boteler, D.
704 H., Singer, H. J., Opgenoorth, H., Schillings, A., Ohtani, S., Gjerloev, J., & Russell, C. T. (2021a).
705 Nighttime magnetic perturbation events observed in Arctic Canada: 3. Occurrence and
706 amplitude as functions of magnetic latitude, local time, and magnetic disturbances. *Space*
707 *Weather*, *19*, e2020SW002526. https://doi.org/10.1029/2020SW002526
708
709 Engebretson, M. J., Ahmed, L. Y., Pilipenko, V. A., Steinmetz, E. S., Moldwin, M. B., Connors, M.
710 G., Boteler, D. H., Weygand, J. M., Coyle, S., Ohtani, S., Gjerloev, J., & Russell, C. T. (2021b).
711 Superposed epoch analysis of nighttime magnetic perturbation events observed in Arctic
712 Canada (2021). *Journal of Geophysical Research: Space Physics, 126*, e2021JA029465.
713 https://doi:10.1029/2021JA029465
714

715 Engebretson, M. J. (2023). Solar Cycle Dependence of Very Large Nighttime Geomagnetic
716 Disturbances (GMDs) Observed in Eastern Arctic Canada: Data [Data set], University of
717 Michigan - Deep Blue Data. https://doi.org/10.7302/275e-da06
718
719 Gannon, J. L., Swidinsky, A., & Xu, Z. (Eds.) (2019). Geomagnetically induced currents from the
720 Sun to the power grid. *Geophysical Monograph Series* (Vol. 244). American Geophysical Union.
721 https://doi.org/10.1002/9781119434412
722
723 Haiducek, J. D., Welling, D. T., Ganushkina, N. Y., Morley, S. K., & Ozturk, D. S. (2017). SWMF
724 Global Magnetosphere Simulations of January 2005: Geomagnetic Indices and Cross-Polar Cap
725 Potential. *Space Weather*, *15*, 1567–1587. https://doi.org/10.1002/2017SW001695
726
727 Hajra, R. (2022). Intense, long-duration geomagnetically induced currents (GICs) caused by
728 intense substorm clusters. *Space Weather, 20, e2021SW002937.*
729 https://doi.org/10.1029/2021SW002937
730
731 Hapgood, M. (2019). The Great storm of May 1921: An exemplar of a dangerous space weather
732 event. *Space Weather*, *17*, 950–975. https://doi.org/10.1029/2019SW002195
733
734 Ieda, A., Nishimura, Y., Miyashita, Y., Angelopoulos, V., Runov, A., Nagai, T., Frey, H. U.,
735 Fairfield, D. H., Slavin, J.A., Vanhamäki, H., Uchino, H., Fujii, R., Miyoshi, Y, & Machida, S. (2016).
736 Stepwise tailward retreat of magnetic reconnection: THEMIS observations of an auroral
737 substorm. *Journal of Geophyical Research: Space Physics*, *121*, 4548–4568.
738 doi:10.1002/2015JA022244.
739
740 Juusola, L., Viljanen, A., Dimmock, A. P., Kellinsalmi, M., Schillings, A., & Weygand, J. M. (2023).
741 Drivers of rapid geomagnetic variations at high latitudes. *Annales Geophysicae, 41*, 13–37.
742 https://doi.org/10.5194/angeo-41-13-2023
743

744 Kappenman, J. G. (2001). An introduction to power grid impacts and vulnerabilities from space
745 weather. In I. A. Daglis (Ed.), Space storms and space weather hazards, NATO science series
746 (series II: Mathematics, physics and chemistry) (Vol. 38, pp. 335–361). Springer Netherlands.
747 https://doi.org/10.1007/978-94-010-0983-6_13
748
749 Kappenman, J. G. (2006). Great geomagnetic storms and extreme impulsive geomagnetic field
750 disturbance events—An analysis of observational evidence including the great storm of May
751 1921. *Advances in Space Research*, *38*(2), 188–199. https://doi.org/10.1016/j.asr.2005.08.055
752
753 Kellinsalmi, M., Viljanen, A., Juusola, L, & Käki, S. (2022). The time derivative of the
754 geomagnetic field has a short memory. *Ann. Geophys., 40,* 545–562.
755 https://doi.org/10.5194/angeo-40-545-2022
756
757 Kim H.-J., Lyons, L. R., Zou, S., Boudouridis, A., Lee, D.-Y., Heinselman, C., & McCready, M.
758 (2009). Evidence that solar wind fluctuations substantially affect the strength of dayside
759 ionospheric convection. *Journal of Geophysical Research, 114,* A11305.
760 doi:10.1029/2009JA014280
761
762 Kwagala, N., Hesse, M., Moretto, T., Tenfjord, P., Norgren, C., Toth, G., Gombosi, T., Kolstø, H.
763 M., and Spinnangr, S. (2020). Validating the Space Weather Modeling Framework (SWMF)
764 for applications in northern Europe: Ground magnetic perturbation validation, *J. Space Weather*
765 *Space Clim., 10, 1–13*. https://doi.org/10.1051/swsc/2020034
766
767 Le, G., Russell, C. T., Petrinec, S. M, & Ginskey, M. (1993). Effect of sudden solar wind dynamic
768 pressure changes at subaurorallLatitudes: Change in magnetic field. *Journal of Geophysical*
769 *Research, 98,* 3983-3990. https://doi.org/10.1029/92ja02397
770
771 Liemohn, M., Ganushkina, N. Y., De Zeeuw, D. L., Rastaetter, L., Kuznetsova, M., Welling, D. T.,
772 et al. (2018). Real-time SWMF at CCMC: Assessing the Dst output from continuous operational
773 simulations. *Space Weather*, *16*(10), 1583–1603. https://doi.org/10.1029/2018SW001953

Love, J. J., Hayakawa, H., & Cliver, E. W. (2019). Intensity and impact of the New York Railroad superstorm of May 1921. *Space Weather*, *17*, 1281–1292. https://doi.org/10.1029/2019SW002250

Lyons, L. R., Kim,1-H.-J., Xing,X., Zou, S., Lee, D. Y., Heinselman, C., Nicolls, M. J., Angelopoulos,V., Larson, D., J. McFadden, J., Runov, A., & Fornacon, K.-H. (2009). Evidence that solar wind fluctuations substantially affect global convection and substorm occurrence. *Journal of Geophysical Research, 114,* A11306. https://doi.org/10.1029/2009JA014281

Lyons, L. R., Nishimura, Y., Kim, H.-J., Donovan, E., Angelopoulos, V., Sofko, G., Nicolls, M., Heinselman, C., J. M. Ruohoniemi, J. M., & Nishitani, N. (2011). Possible connection of polar cap flows to pre- and post-substorm onset PBIs and streamers. *Journal of Geophysical Research, 116,* A12225. https://doi.org/10.1029/2011JA016850

Lyons, L. R., Nishimura, Y., Donovan, E., & Angelopoulos, V. (2013). Distinction between auroral substorm onset and traditional ground magnetic onset signatures. *Journal of Geophysical Research: Space Physics, 118*, 4080–4092. https://doi.org/10.1002/jgra.50384

Mac Manus, D. H., Rodger, C. J., Dalzell, M., Renton, A., Richardson, G. S., Petersen, T., & Clilverd, M. A. (2022). Geomagnetically induced current modeling in New Zealand: Extreme storm analysis using multiple disturbance scenarios and industry provided hazard magnitudes. *Space Weather*, *20*, e2022SW003320. https://doi.org/10.1029/2022SW003320

Marshall, R. A., Smith, E.A., Francis, M. J., Waters, C. L., & Sciffer, M. D. (2011). A preliminary risk assessment of the Australian region power network to space weather. *Space Weather, 9*, S10004. https://doi.org/10.1029/2011SW000685

McCuen, B. A., Moldwin, M. B., & Engebretson, M. J. (2021). Characterization of transient-large-amplitude geomagnetic perturbation events. *Geophysical Research Letters, 48,* e2021GL094076. https://doi.org/10.1029/2021GL094076

McCuen, B. A., Moldwin, M. B., Engebretson, M. J., Weygand, J. M., [& Nishimura, Y.] (2023). A statistical analysis of high-frequency transient-large-amplitude geomagnetic disturbances. Submitted to the *Journal of Geophysical Research: Space Physics.* https://doi.org/10.1029/2023JA031587

Milan, S. E., Imber, S. M., Fleetham, A. L., & Gjerloev, J. (2023). Solar cycle and solar wind dependence of the occurrence of large *dB*/*dt* events at high latitudes. *Journal of Geophysical Research: Space Physics*, *128*, e2022JA030953. https://doi.org/10.1029/2022JA030953

Molinski, T. S., Feero, W. E., & Damsky, B. L. (2000). Shielding grids from solar storms. *IEEE Spectrum*, *37*(11), 55–60. https://doi.org/10.1109/6.880955

Morley, S. K. (2020). Challenges and opportunities in magnetospheric space weather prediction. *Space Weather*, *18*, e2018SW002108. https://doi.org/10.1029/2018SW002108

Mursula, K., Qvick, T., Holappa, L., & Asikainen, T. (2022). Magnetic storms during the space age: Occurrence and relation to varying solar activity. *Journal of Geophysical Research: Space Physics*, *127*, e2022JA030830. https://doi.org/10.1029/2022JA030830

Nakamura, R., Baumjohann, W., Panov, E., Petrukovich, A. A., Angelopoulos, V., Volwerk, M., Magnes, W., Nishimura, Y., Runov, A., Russell, C. T., Weygand, J. M., Amm, O., Auster, H.-U., J. Bonnell, J., H. Frey, H., Larson, D., & McFadden, J. (2011). Flux transport, dipolarization, and current sheet evolution during a double-onset substorm. *Journal of Geophysical Research*, *116*, A00I36. doi:10.1029/2010JA015865

831 Newell, P. T., & Gjerloev, J. W. (2011a). Evaluation of SuperMAG auroral electrojet indices as
832 indicators of substorms and auroral power. *Journal of Geophysical Research*, *116*, A12211.
833 https://doi.org/10.1029/2011JA016779
834
835 Newell, P. T., & Gjerloev, J. W. (2011b). Substorm and magnetosphere characteristic scales
836 inferred from the SuperMAG auroral electrojet indices. *Journal of Geophysical Research*, *116*,
837 A12232. https://doi.org/10.1029/2011JA016936
838
839 Ngwira, C. M., Sibeck, D., Silveira, M. D. V., Georgiou, M., Weygand, J. M., Nishimura, Y., and
840 Hampton, D. (2018). A study of intense local dB/dt variations during two geomagnetic storms,
841 *Space Weather, 16,* 676–693. https://doi.org/10.1029/2018SW001911
842
843 Ngwira, C. M., & Pulkkinen, A. A. (2019). An introduction to geomagnetically induced currents.
844 In J. L. Gannon, A. Swidinsky, & Z. Xu (Eds.), *Geomagnetically induced currents from the Sun to*
845 *the power grid, Geophysical Monograph Series* (Vol. 244, pp. 3–13). American Geophysical
846 Union. https://doi.org/10.1002/9781119434412.ch1
847
848 Nishimura, Y., L. R. Lyons, L. R., Shiokawa, K., Angelopoulos, V., Donovan, E. F., & and Mende, S.
849 B. (2013). Substorm onset and expansion phase intensification precursors seen in polar cap
850 patches and arcs. *Journal of Geophysical Research: Space Physics, 118,* 2034–2042.
851 doi:10.1002/jgra.50279
852
853 Oliveira, D. M., Arel, D., Raeder, J., Zesta, E., Ngwira, C. M., Carter, B. A., Yizengaw, E., Halford.,
854 A. J., Tsurutani, B. T., & Gjerloev, J. (2018). Geomagnetically induced currents caused by
855 interplanetary shocks with different impact angles and speeds. *Space Weather*, *16*, 636–647.
856 https://doi.org/10.1029/2018SW001880
857

Pilipenko, V., Kozyreva, O., Hartinger, M., Rastaetter, L., & Sakharov, Y. (2023). Is the Global MHD Modeling of the Magnetosphere Adequate for GIC Prediction: The May 27–28, 2017 Storm. *Cosmic Research, 2023, 61, 120–132.* ISSN 0010-9525

Pulkkinen, A., Amm, O., Viljanen, A., & BEAR Working Group (2003). Ionospheric equivalent current distributions determined with the method of spherical elementary current systems. *Journal of Geophysical Research, 108,* 1053. https://doi.org/10.1029/2001JA005085

Pulkkinen, A., Rastatter, L., Kuznetsova, M., Singer, H., Balch, C., Weimer, D., Toth, G., Ridley, A., Gombosi, T., Wiltberger, M., Raeder, M., and Weigel, R. (2013). Community-wide validation of geospace model ground magnetic field perturbation predictions to support model transition to operations. *Space Weather,* 11, 369–385. https://doi.org/10.1002/swe.20056

Pulkkinen, A., Bernabeu, E., Thomson, A., Viljanen, A., Pirjola, R., Boteler, D., et al. (2017). Geomagnetically induced currents: Science, engineering, and applications readiness. Space Weather, 15(7), 828–856. https://doi.org/10.1002/2016SW001501

Pulkkinen, T. I., Brenner, A., Al Shidi, Q., & Toth, G. (2022). Statistics of geomagnetic storms: Global simulations perspective. *Frontiers in Astronomy and Space Sciences*, *9*. https://doi.org/10.3389/fspas.2022.972150

Reiter,K., Guillon, S., Connors, M., & Jackel, B. (2021. Statistics of large impulsive magnetic events in the auroral zone. *Journal of Space Weather and Space Climate 11*, 44. https://doi.org/10.1051/swsc/2021029

Schillings, A., Palin, L., Opgenoorth, H. J., Hamrin, M., Rosenqvist, L., Gjerloev, J. W., Juusola, L., and Barnes, R. (2022). Distribution and occurrence frequency of dB/dt spikes during magnetic storms 1980–2020. *Space Weather*, *20*, e2021SW002953. https://doi.org/10.1029/2021SW002953

Tsurutani, B. T., & Gonzalez. W. D. (1987). The cause of high intensity long duration continuous AE activity (HILDCAAs): Interplanetary Alfven wave trains, *Planet. Space Sci., 35,* 405–412. https://doi.org/10.1016/0032-0633(87)90097-3

Tsurutani, B. T., Gonzalez, W. D., Gonzalez, A. L. C, Tang, F., Arballo, J. K., & Okada, M. (1995). Interplanetary origin of geomagnetic activity in the declining phase of the solar cycle. *Journal of Geophysical Research, 100, A11.* https://doi.org/10.1029/95JA01476

Tsurutani, B. T., Gonzalez, W. D., Lakhina, G.S., & Alex, S. (2003). The extreme magnetic storm of 1–2 September 1859. *Journal of Geophysical Research, 108,* 1268. https://doi.org/10.1029/2002JA009504

Tsurutani, B. T., Gonzalez, W. D., Gonzalez, A. L. C., Guarnieri, F. L., Gopalswamy, N., Grande, M., Kamide, Y., Kasahara, Y., Lu, G., Mann, I., McPherron, R., Soraas, F., & Vasyliunas, V. (2006). Corotating solar wind streams and recurrent geomagnetic activity: A review. *Journal of Geophysical Research, 111*, A07S01. https://doi.org/10.1029/2005JA011273

Tsurutani, B. T., Echer, E., Guarnieri, F. L., and Gonzalez, W. D. (2011), The properties of two solar wind high speed streams and related geomagnetic activity during the declining phase of solar cycle 2. *Journal of Atmospheric and Solar-Terrestrial Physics, 73,* 164-177. https://doi.org/10.1016/j.jastp.2010.04.003

Tsurutani, B. T., Zank, G. P., Sterken, V. J., Shibata, K., Nagai, T., Mannucci, A. J., Malaspina, D. M., Lakhina, G. S., Kanekal, S. G., Hosokawa, K., Horne, R. B., Hajra, R., Glassmeier, K.-H., Gaunt, C. T., Chen, P.-F., & Syun-Ichi Akasofu, S.-I. (2022). *Space Plasma Physics: A Review.* Accepted for publication in *IEEE Transactions on Plasma Science*

913 Viljanen, A. (1997). The relation between geomagnetic variations and their time derivatives and
914 implications for estimation of induction risks. *Geophysical Research Letters*, *24*, 631–634.
915 https://doi.org/10.1029/97GL00538
916
917 Viljanen, A., Nevanlinna, H., Pajunpaa, K., & Pulkkinen, A. (2001). Time derivative of the
918 horizontal geomagnetic field as an activity indicator. *Annales Geophysicae*, *19*, 1107–1118.
919 https://doi.org/10.5194/angeo-19-1107-2001
920
921 Viljanen, A., E. I. Tanskanen, E. I. and Pulkkinen, A. (2006). Relation between substorm
922 characteristics and rapid temporal variations of the ground magnetic field. *Annales*
923 *Geophysicae, 24,* 725-733. https://doi.org/10.5194/angeo-24-725-2006
924
925 Viljanen, A., Pirjola, R., Prácser, E., Ahmadzai, S., & Singh, V. (2013). Geomagnetically induced
926 currents in Europe: Characteristics based on a local power grid model. *Space Weather*, *11*,
927 575–584, https://doi.org/10.1002/swe.20098.
928
929 Weygand, J. M., Amm, O., Viljanen, A., Angelopoulos, V., Murr, D., Engebretson, M. J., et al.
930 (2011). Application and validation of the spherical elementary currents systems technique for
931 deriving ionospheric equivalent currents with the North American and Greenland
932 ground magnetometer arrays. *Journal of Geophysical Research*, *116*, A03305.
933 https://doi.org/10.1029/2010JA06177
934
935 Weygand, J. M., Engebretson, M. J., Pilipenko, V. A., Steinmetz, E. S., Moldwin, M. B., Connors,
936 M. G., et al. (2021). SECS analysis of nighttime magnetic perturbation events observed in Arctic
937 Canada. *Journal of Geophysical Research: Space Physics*, *126*, e2021JA029839.
938 https://doi.org/10.1029/2021JA029839
939

940 Woodroffe, J. R., Morley, S. K., Jordanova, V. K., Henderson, M. G., Cowee, M. M., & Gjerloev, J.
941 (2016). The latitudinal variation of geoelectromagnetic disturbances during large (*Dst*≤−100 nT)
942 geomagnetic storms. *Space Weather*, *14*, 668–681. https://doi.org/10.1002/2016SW001376
943
944 Yermolaev, Y.I., Nikolaeva, N.S., Lodkina, I.G., & Yermolaev, M. Yu. (2009). Catalog of large-
945 scale solar wind phenomena during 1976–2000. *Cosmic Research 47*, 81–94.
946 https://doi.org/10.1134/S0010952509020014
947
948 Zou, Y., Nishimura, Y., Lyons, L. R., Donovan, E. F., Shiokawa, K., Ruohoniemi, J. M., McWilliams,
949 K. A., & Nishitani, N. (2015). Polar cap precursor of nightside auroral oval intensifications using
950 polar cap arcs, *Journal of Geophysical Research: Space Physics, 120,* 10,698-10,711.
951 https://doi.org:10.1002/2015JA021816
952
953 Zou, Y., Dowell, C., Ferdousi, B., Lyons, L. R., & Liu, J. (2022). Auroral drivers of large dB⁄dt
954 during geomagnetic storms. *Space Weather*, *20*, e2022SW003121.
955 https://doi.org/10.1029/2022SW003121
956

Table 1. Locations of the magnetometer stations used in this study. Geographic and corrected geomagnetic (CGM) latitude and longitude are shown, as well as the universal time (UT) of local magnetic midnight. Distances between nearest-neighbor pairs of stations are also presented.

Array	Station	Code	Geog. Lat.	Geog. Lon.	CGM Lat.	CGM Lon.	UT of Mag Midnight
MACCS	Repulse Bay	RBY	66.5°	273.8°	75.2°	-12.8°	05:47
	Cape Dorset	CDR	64.2°	283.4°	72.7°	3.0°	04:58
	Pangnirtung	PGG	66.1°	294.2°	73.3°	19.8°	03:53
AUTUMNX	Salluit	SALU	62.2°	284.3°	70.7°	4.1°	04:54
	Kuujjuarapik	KJPK	55.3°	282.2°	64.7°	0.2°	05.06

Interstation Distances:		
	RBY-CDR	512 km
	CDR-PGG	546 km
	CDR-SALU	226 km
	SALU-KJPK	776 km

Note: CGM coordinates were calculated for epoch 2015, using http://sdnet.thayer.dartmouth.edu/aacgm/aacgm_calc.php#AACGM .

Table 2. Number of available station days, ≥ 6 and ≥ 20 nT/s GMD events, and percent of GMDs per station day observed from 2011 through 2022.

Year	2011	2012	2013	2014	2015	2016	2017	2018	2019	2020	2021	2022
Station Days	452	587	767	1213	1682	1346	1542	1677	1520	1377	1328	1672
≥6 nT/s GMDs	69	82	88	131	611	550	745	460	398	289	330	528
% ≥6 nT/s/Day	15.3	14.0	11.5	10.8	36.3	40.9	48.3	27.4	26.2	21.0	24.9	31.6
≥20 n/s GMDs	0	2	3	0	14	11	18	6	5	1	3	9
% ≥20 nT/s/Day	0	0.34	0.39	0	0.83	0.82	1.17	0.36	0.33	0.07	0.23	0.54

Table 3. Distribution of 71 ≥ 20 nT/s GMD events as a function of year and solar wind velocity (Vsw) observed from 2011 through 2022. * - No Vsw data were available for 1 day in 2017 in the OMNI database.

Year	Vsw range					
	300-399	400-499	500-599	600-699	700-799	Total
2011						0
2012	1				1	2
2013			1	2		3
2014						0
2015	1		1	12		14
2016	2	2		6	1	11
2017			3	11	3	17*
2018	1	2	2	1		6
2019		1	3		1	5
2020			1			1
2021		1	1		1	3
2022		5	3		1	9

Table 4. Distribution of 71 ≥ 20 nT/s GMD events as a function of year, solar wind velocity (Vsw) below and above 500 km/s, and the presence or absence of rapid solar wind pressure (Psw) increases of 1.5 nT or more, from 2011 through 2022. * - No Vsw data were available for 1 day in 2017 in the OMNI database.

Year	2011	2012	2013	2014	2015	2016	2017	2018	2019	2020	2021	2022	Total
Vsw < 500 km/s													
P rising	0	1	0	0	0	1	0	1	1	0	1	1	6
P steady	0	0	0	0	1	3	0	2	0	0	0	4	10
Vsw > 500 km/s													
P rising	0	0	1	0	6	1	3	0	1	0	1	0	13
P steady	0	1	2	0	7	6	14	3	3	1	1	4	42
Total	0	2	3	0	14	11	17*	6	5	1	3	9	71

Table 5. Distribution of ≥ 20 nT/s GMD events as a function of geomagnetic storm phase. Definitions for the four storm categories are taken from Mursula et al. (2022).

Storm Category	Range of Dst Minimum	Main Phase	Recovery Day 1	Recovery Days 2-5	Number of Events
SI/SC					4
Major	≤ -200 nT	0	0	3	3
Intense	-200 ≤ -100 nT	1	2	2	5
Moderate	-99 ≤ -50 nT	11	11	8	30
Weak	-49 ≤ -30 nT	6	11	3	20
Quiet	> -29 nT				10

Table 6. Distribution of GMD events with amplitude ≥ 20 nT/s observed from 2011 through 2022, sorted into categories in the Yermolaev et al. (2009) list. Events in the categories "Ejecta," "Magnetic Cloud," and "Sheath" are all included here under the CME heading. Both CIR and CME events are broken down further using the "Fast" and "Slow" categories (>450 or <450 km/s, respectively) into CME-F, CME-S, CIR-F and CIR-S in this table. Events are listed as "FAST" or "SLOW" only if they do not also fall into the above IS, CME, or CIR categories.

Year	2011	2012	2013	2014	2015	2016	2017	2018	2019	2020	2021	2022	Total
IS		1						1					2
CME-S					1	3			1				5
CME-F		1	2		5		4		1		1	2	16
CIR-S						1		1					2
CIR-F			1			1	3	1				3	9
FAST					8	6	11	3	3	1	2	4	38
SLOW													0

Table 7. Distribution of >20 nT/s GMD events as a function of year and SYM/H value observed from 2011 through 2022.

Year	SYM/H Range												
	-100 -91	-90 -81	-80 -71	-70 -61	-60 -51	-50 -41	-40 -31	-30 -21	-20 -11	-10 -1	0 9	Total
2011												0
2012				1							1	2
2013						1	1			1		3
2014												0
2015				2	3	3	3	3				14
2016	1	1		1			3	2	3			11
2017		1		1	1	1	4	4	6			18
2018						2	3			1		6
2019				1			3	1				5
2020									1			1
2021							1		2			3
2022				2	1		3	2	1			9
Total	1	2		8	5	7	21	12	13	2	1	72

Figures

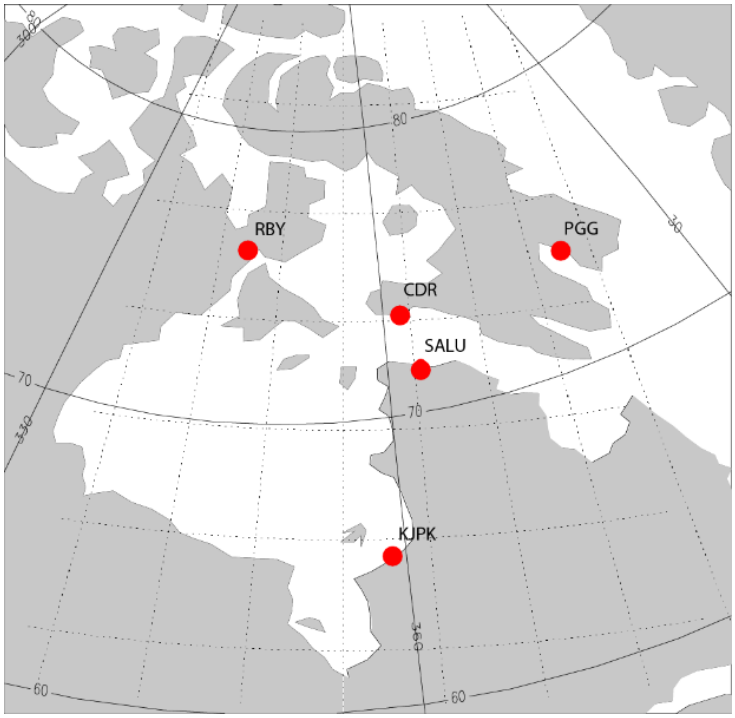

Figure 1. Map of ground magnetometer stations used for this study. Selected latitude and longitude lines in geomagnetic coordinates are shown.

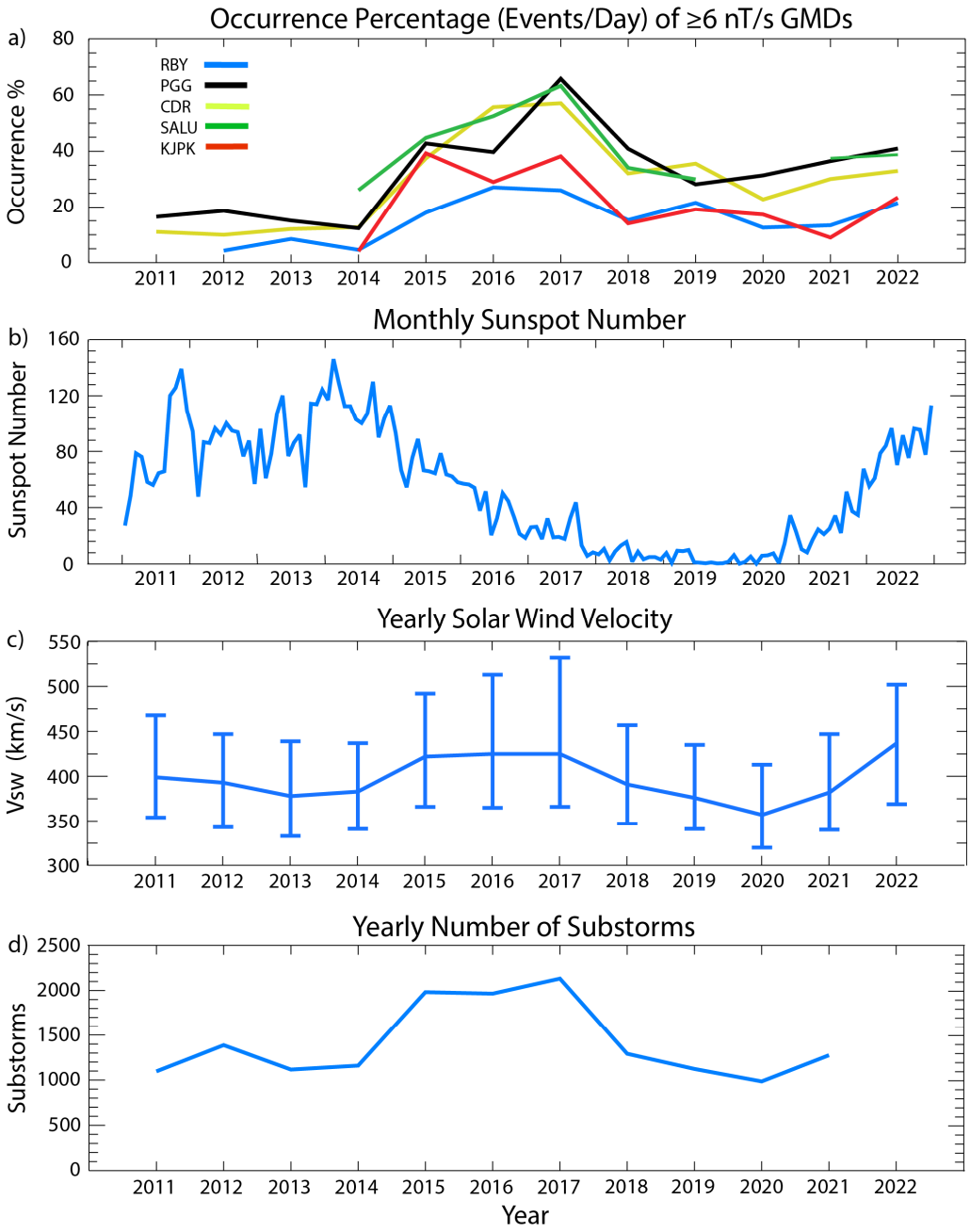

Figure 2. (a) Yearly occurrence percentages (events/station day) of ≥ 6 nT/s GMDs observed at 5 sites in Eastern Arctic Canada from 2011 through 2022. (b) Monthly sunspot numbers from January 2011 through December 2022. (c) Yearly medians and 25th and 75th percentile values (lower and upper bars) of the solar wind velocity and (d) Yearly number of substorm onsets, respectively, from 2011 through 2022.

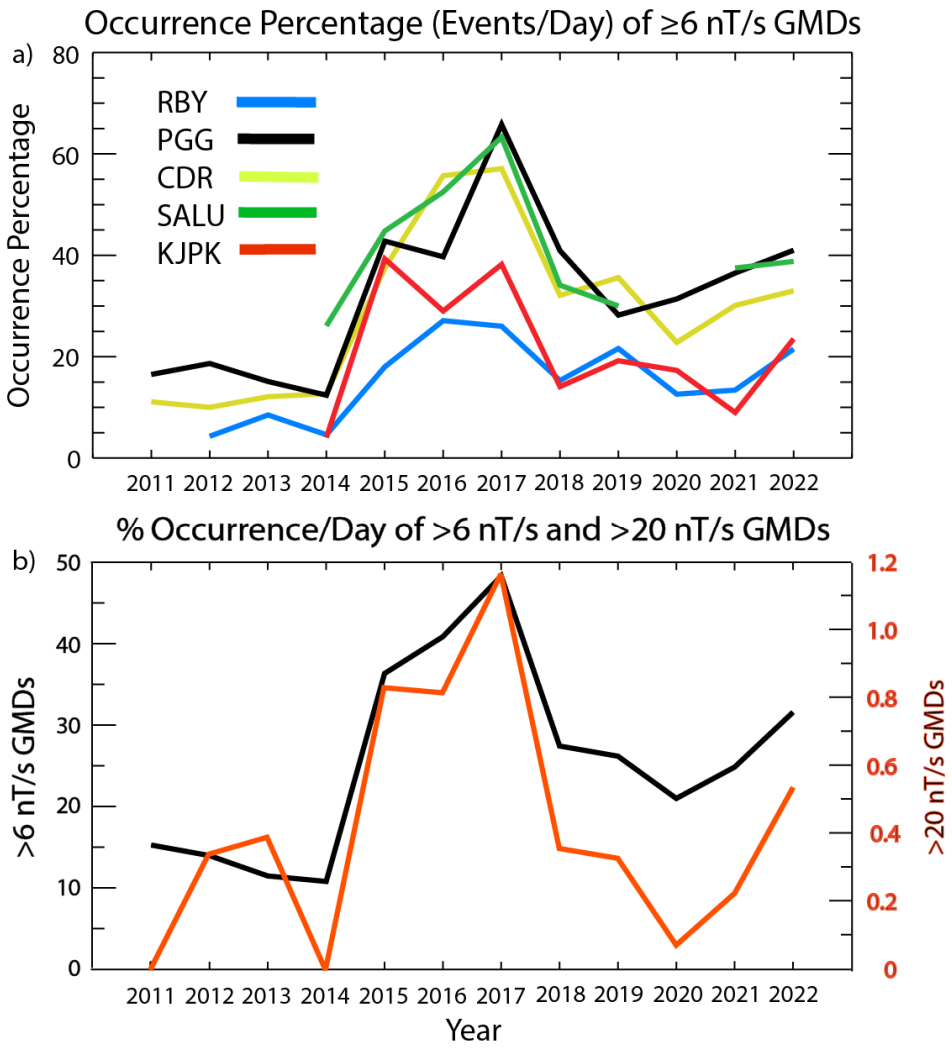

Figure 3. (a) Yearly occurrence percentages (events/station day) of ≥ 6 nT/s GMDs observed at each of five sites in Eastern Arctic Canada from 2011 through 2022. (b) Yearly summed occurrence percentages at all 5 sites (events/station day) of ≥ 6 nT/s GMDs (black trace and left vertical axis) and ≥ 20 nT/s GMDs (orange trace and right vertical axis).

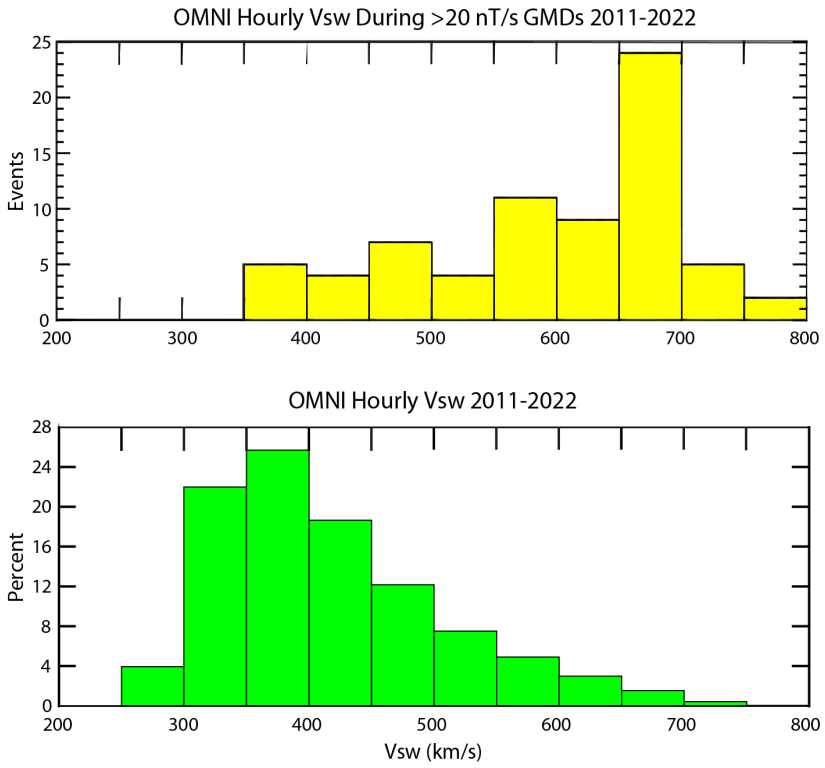

Figure 4. (a) Histogram of the distribution of hourly averaged solar wind velocities (Vsw) during ≥ 20 nT/s GMD events. (b) Histogram of the distribution of hourly averaged solar wind velocities (Vsw) from 2011 through 2022.

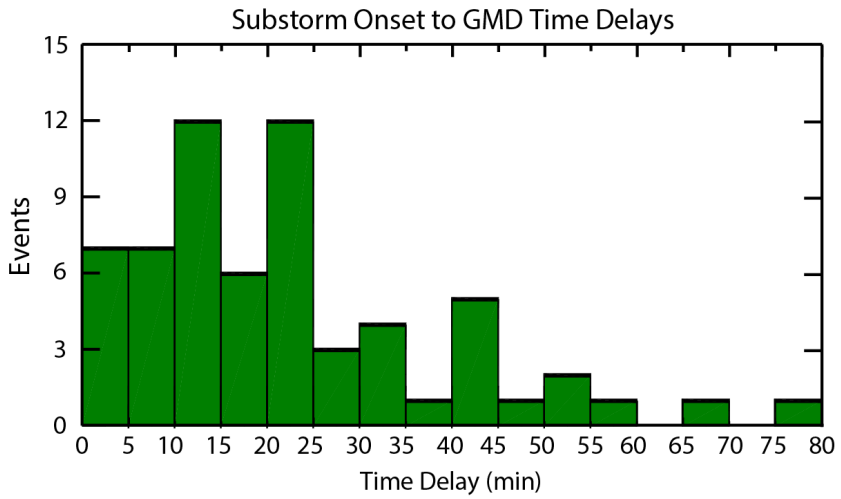

Figure 5. Histogram of the number of ≥ 20 nT/s GMD events as a function of their time delay since the most recent substorm onset listed in the SuperMAG Newell and Gjerloev (2011) catalog.

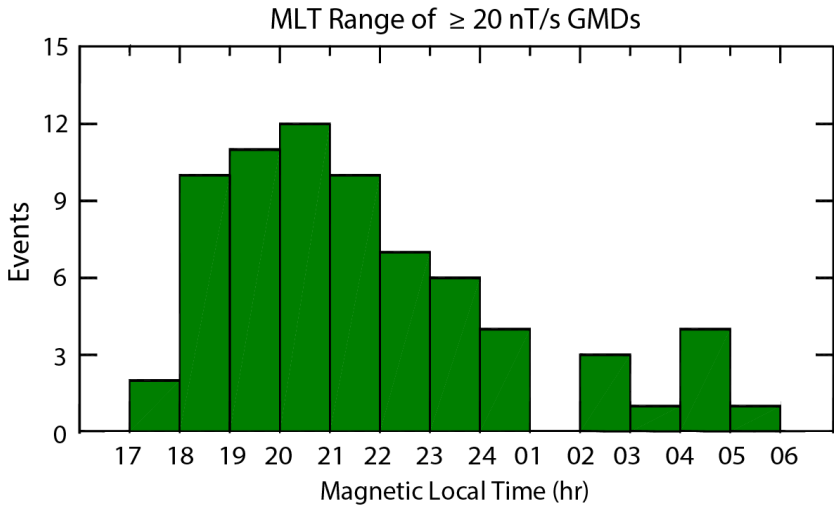

1140

1141

1142 Figure 6. Histogram of the number of ≥ 20 nT/s GMD events as a function of magnetic local

1143 time (MLT).

1144

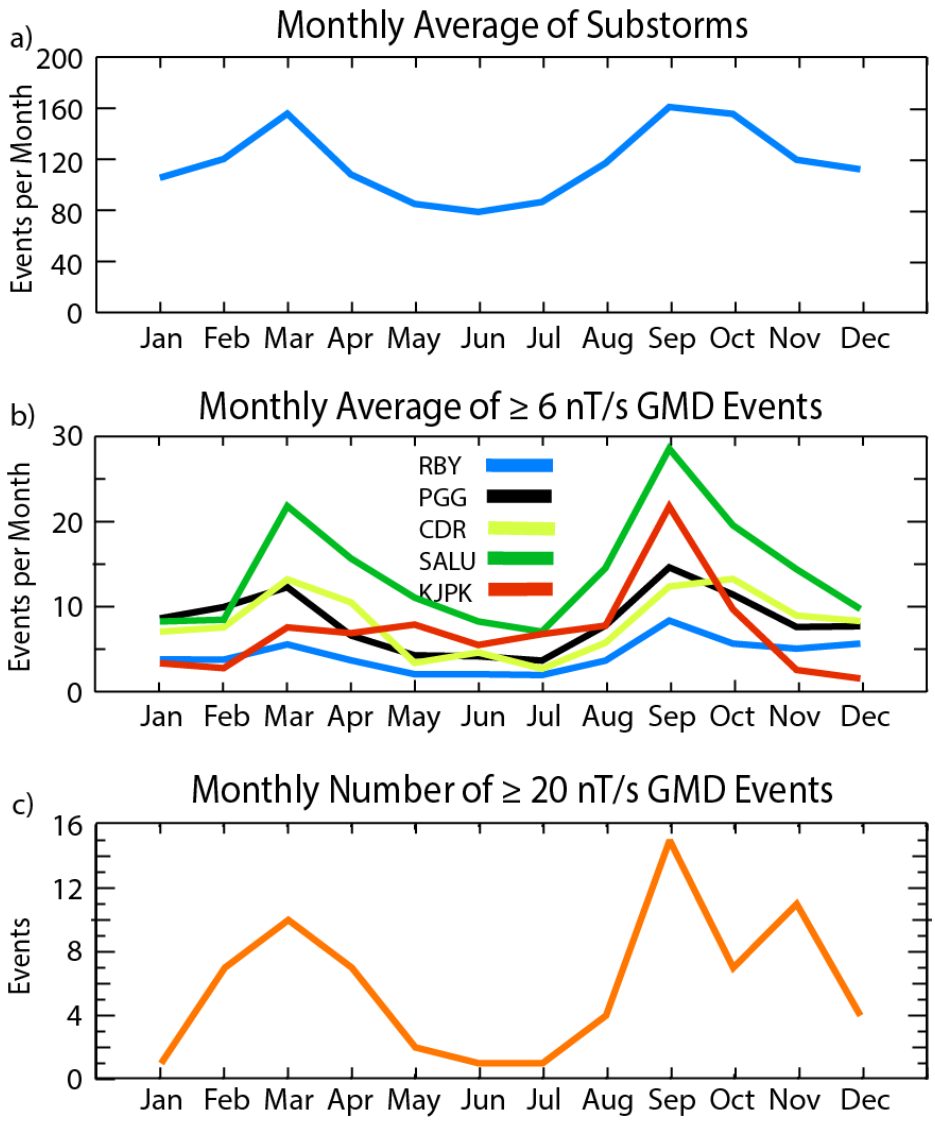

Figure 7. Monthly distributions of substorms and GMDs. Panel a shows the average number of events per month from 2011 through 2021 (no year 2022 substorm list was available on SuperMAG as of 4/12/2023). Panel b shows the weighted monthly average number of ≥ 6 nT/s GMDs from 2011 through 2021, and panel c shows the distribution of ≥ 20 nT/s GMDs from 2011 through 2022.

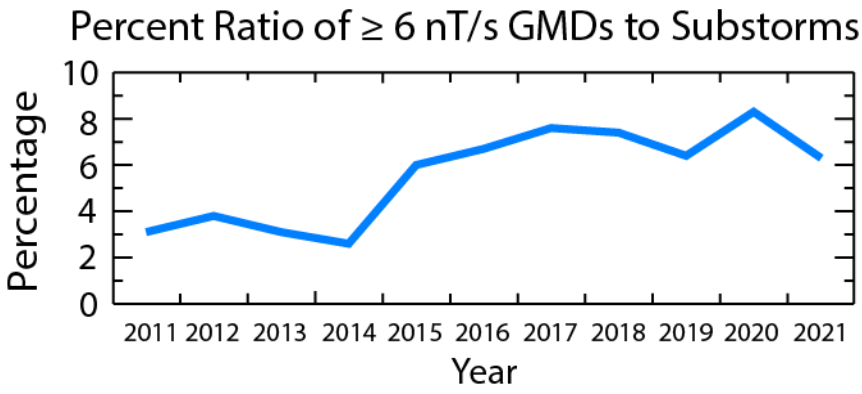

Figure 8. Plot of the percentage ratio of yearly ≥ 6 nT/s GMDs to the yearly number of substorms after taking into account the less than complete magnetometer coverage during several years at individual stations,

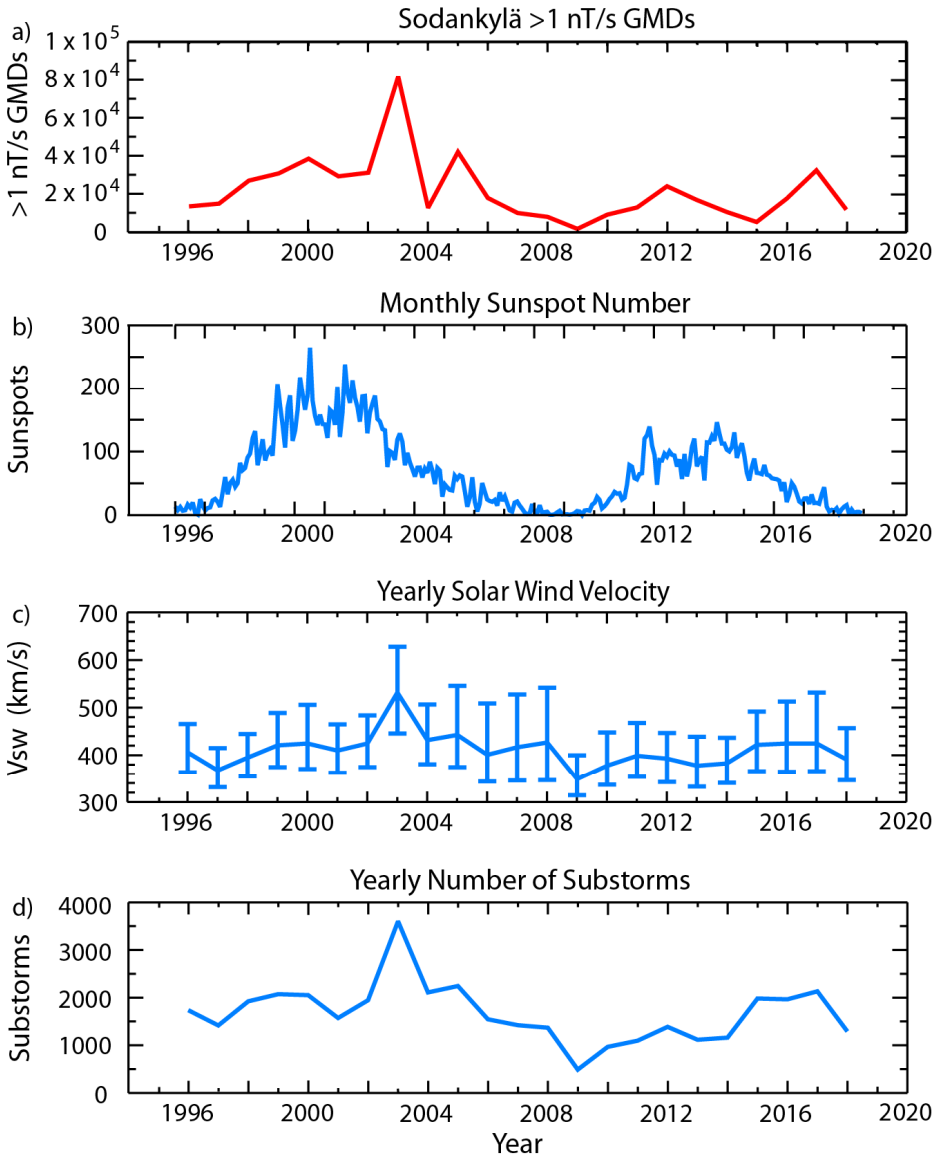

Figure 9. (a) Yearly numbers of ≥ 1 nT/s GMDs observed at Sodankylä, Finland from 1996 through 2018. (b) Monthly sunspot numbers from January 1996 through December 2018. (c) Yearly medians and 25th and 75th percentile values (lower and upper bars) of the solar wind velocity and (d) Yearly averages of the number of substorm onsets, respectively, from 1996 through 2018, again taken from the SuperMAG substorm list.

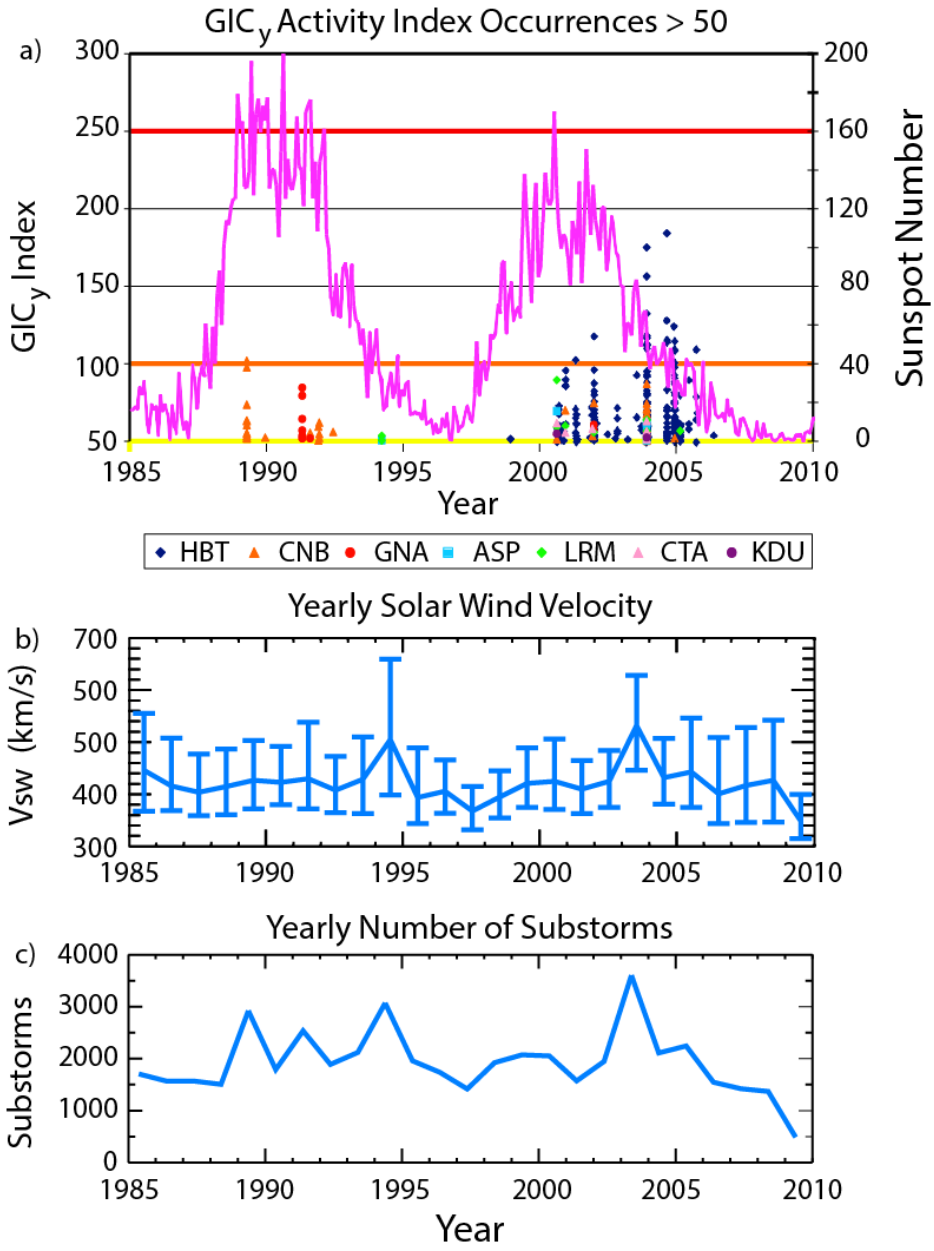

Figure 10. (a): A copy of Figure 7 of Marshall et al. (2011), showing GICy indices > 50 from magnetometer locations across Australia along with the solar sunspot number (pink), from 1985 through 2009. The horizontal yellow, orange, and red lines are the lower limit thresholds for the "low," "moderate," and "high" threat levels defined in that study. (b) Yearly medians and 25th and 75th percentile values (lower and upper bars) of the solar wind velocity and (c) Yearly averages of the number of substorm onsets, respectively, from 1985 through 2009.